# GENERALISED PHASE DIVERSITY WAVEFRONT SENSING[1]

**Heather I. Campbell**
**Sijiong Zhang**
**Aurelie Brun**[2]
**Alan H. Greenaway**
*Heriot-Watt University, School of Engineering and Physical Sciences, Edinburgh EH14 4AS UK*

## ABSTRACT

Phase Diversity (PD) is an algorithm for the reconstruction of a wavefront using image data from two planes symmetrically placed about the plane containing the wavefront. We have investigated the generalisation of this concept, which currently uses defocus, to allow any form of aberration to be used as the diversity kernel.

This Generalised Phase Diversity (GPD) will be explained, and the symmetry conditions for a suitable aberration kernel will be given. We will discuss future development of the GPD method, and present some preliminary results from a wavefront sensor built using this concept. We will also discuss the range of possible applications for a GPD wavefront sensor and its advantages over the current defocus-only PD wavefront sensor.

## 1. INTRODUCTION

Phase Diversity (PD) may be used as a method for wavefront reconstruction and phase retrieval, using image data from a pair of planes symmetrically placed about the wavefront to be determined. Intensity images captured either side of the wavefront, and perpendicular to the optic axis, may be obtained in a number of ways. These can include physical displacement of the image plane [1], vibrating spherically distorted mirrors [2], beam splitters and folded optical paths. Blanchard et al [3] used off-axis Fresnel zone plates as a method of simultaneous multiplane imaging using a quadratically distorted diffractive optical element (DOE) to apply the diversity, and to display the phase diverse intensity images on a single CCD plane. The images in each diffraction order represent a different level of defocus, and simulate propagation over distances determined by the focal length of the grating. Fig 1 illustrates schematically how the difference in intensity between the two image planes provides information about the shape of the wavefront. Portions of the wavefront that are locally concave will propagate towards a focus and there will be an increase in intensity at this point on the second plane. Portions that are locally convex will continue to diverge and produce spots of lower intensity on the second plane. In this implementation PD and curvature sensing are essentially the same [3].
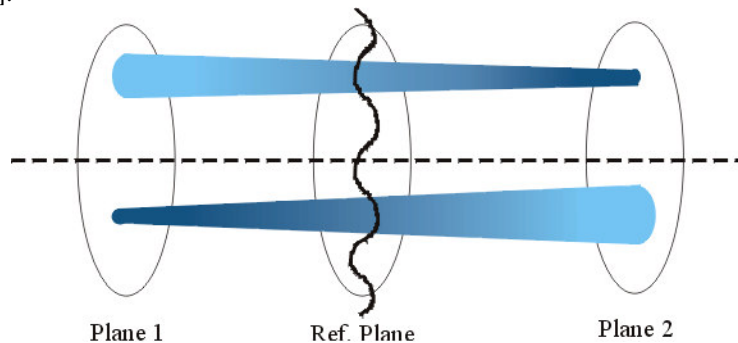


Fig 1. Schematic showing the relationship between intensity and wavefront curvature

[2] Visiting 'stage' student from the Ecole Polytechnique d'Orleans, BP 6744, F45067, Orleans Cedex 2, France

The difference between the intensity images is therefore an approximation to the axial intensity derivative and may be used in the Intensity Transport Equation (ITE) with a Green's function solution to reconstruct the wavefront under test [4, 5]. This defocus based PD (DPD) wavefront sensor has been shown to provide real-time wavefront reconstruction with sub-nanometre accuracy [6].

However, assumptions imposed on the wavefront by use of the Green's function solution limit the performance of a wavefront sensor based on this method. The assumptions are that the wavefront, and its first derivative (the slope), must be everywhere continuous within the pupil and also that the input wavefront has uniform intensity. This limitation means that reconstruction will be poor when used with discontinuous or scintillated wavefronts. It also potentially excludes the use of pixellated wavefront modulators, such a liquid crystals, which are lightweight, versatile and cost effective [7, 8]. The DPD sensor, when used with the Green's function algorithm, are poorly suited for metrology of segmented telescope mirrors and integrated circuitry, and real-time polishing applications where a rough surface illuminated by a laser would cause laser speckle. These are just some of the examples of applications for which we would like to develop a suitable sensor through generalisation of the DPD method.

Generalised Phase Diversity (GPD) is a technique that would use aberration functions, other than defocus, in a DOE. Combined with a different data analysis technique this will provide a wavefront sensor that mitigates some of the limitations of the DPD sensor, and can be applied to a wider range of applications.

## 2. GENERALISED PHASE DIVERSITY

Generalised Phase Diversity will use a pair of intensity image. In GPD the wavefront will be convolved with different, but related, aberration functions to provide the phase diverse data for wavefront sensing. These aberration functions will be programmed into a DOE and the images will be recorded on a single CCD plane as in the DPD case. This is demonstrated in Fig 2. The system can be designed to take the images in the pupil plane to preserve the convenient 1-1 mapping of the error on the wavefront with its position on the pupil.
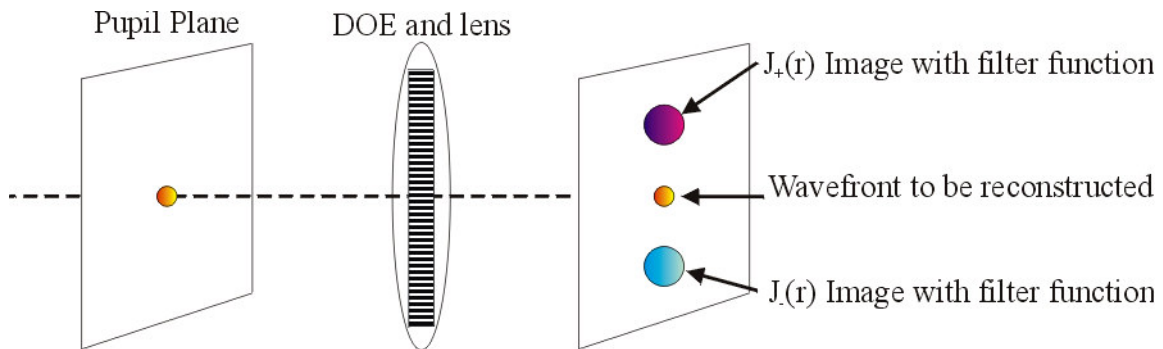


Fig 2. The intensity images in the ±1 diffraction orders are convolved with different, but related, aberration functions produced by the DOE.

## 2.1 NECESSARY AND SUFFICIENT CONDITIONS

To decide on suitable aberration function for the GPD sensor we must first establish the necessary and sufficient conditions for use as a null sensor. A null sensor should only generate an error signal when the test wavefront is distorted. Therefore, sufficient condition for a null sensor is that it should generate no output for plane wavefronts, and an error signal when distortion is present. For the necessary conditions we must look at the symmetry conditions an aberration function must possess in order to generate a useful signal. For convenience we do this by examining the properties of the filter function (i.e. the Fourier Transform (FT) of the aberration function).

As shown in [9], appropriate symmetry conditions that the diversity function should have real $R(\xi)$ and imaginary $I(\xi)$ parts showing the following properties:

1.  The filter function must be complex. If either the real, $R(\xi)$, or imaginary, $I(\xi)$, part of the filter function is zero $\forall \xi$ then the error signal will be zero for all input wavefronts.

2.  $R(\xi)$ and $I(\xi)$ must have the same symmetry. They can both be either odd, or even, but they must be the same. Mixed symmetry (where one of $R(\xi)$ and $I(\xi)$ is odd and one is even) will mean that the sensor produces an error signal whether the input wavefront is distorted or not.

Therefore it can be concluded that for filter functions where $R(\xi)$ and $I(\xi)$ share the same symmetry, this function can be used in the DOE to create a null sensor. This filter function can be constructed from pure Zernike polynomials, combinations of Zernikes, or indeed any function that satisfies the symmetry conditions. The null sensor design is not limited to defocus, as in the DPD case. It is this generalisation of suitable diversity functions that we refer to as Generalised Phase Diversity. We note that all Zernike polynomials which, when expressed in polar form, have the radius $\rho$ raised to an even power and even multiples of the angle $\theta$ satisfy the symmetry conditions for a GPD sensor.

## 2.2 THE ERROR SIGNAL

Equation 1 shows the form of the error signal when a filter function with suitable symmetries is used:

$$
\frac{d(r)}{2i} =
$$

$$
\int d\xi\, H(\xi)\, I(\xi) \exp(-ir\xi) \int d\xi'\, A^*(\xi')\, R(\xi') \exp(ir\xi') - \int d\xi\, A(\xi)\, R(\xi) \exp(-ir\xi) \int d\xi'\, H^*(\xi')\, I(\xi') \exp(ir\xi')
$$

$$
+ \int d\xi\, A(\xi)\, I(\xi) \exp(-ir\xi) \int d\xi'\, H^*(\xi')\, R(\xi') \exp(ir\xi') - \int d\xi\, H(\xi)\, R(\xi) \exp(-ir\xi) \int d\xi'\, A^*(\xi')\, I(\xi') \exp(ir\xi')
$$

$$(1)$$

Where $d(r)$ is the difference between the intensity images in the $\pm 1$ diffraction orders. $H(\xi)$ and $A(\xi)$ are the Hermitian and Anti-Hermitian components of the transform of the input wavefront respectively. $H(\xi)$ being the transform of the purely real parts of the input wavefront and $A(\xi)$ being the transform of the purely imaginary parts. $R(\xi)$ and $I(\xi)$ are the real and imaginary parts of the complex filter function with whose Fourier transform the input wavefront is convolved. Note that the error signal is purely real since the right hand side of equation 1 is purely imaginary because it is the difference of complex conjugates. Note that $\exists$ one, and only one, form of non-flat wavefront that does not lead to an error signal according to this analysis - a $\pi$ discontinuity equivalent to a change of sign in a real-valued function.

## 2.3 ERROR SENSE AND LOCATION

The conditions detailed in 2.1 show that the PSF must be complex since it is the FT of a function whose real and imaginary parts are either both odd or both even. We have plotted some 1-d examples of this using Matlab:
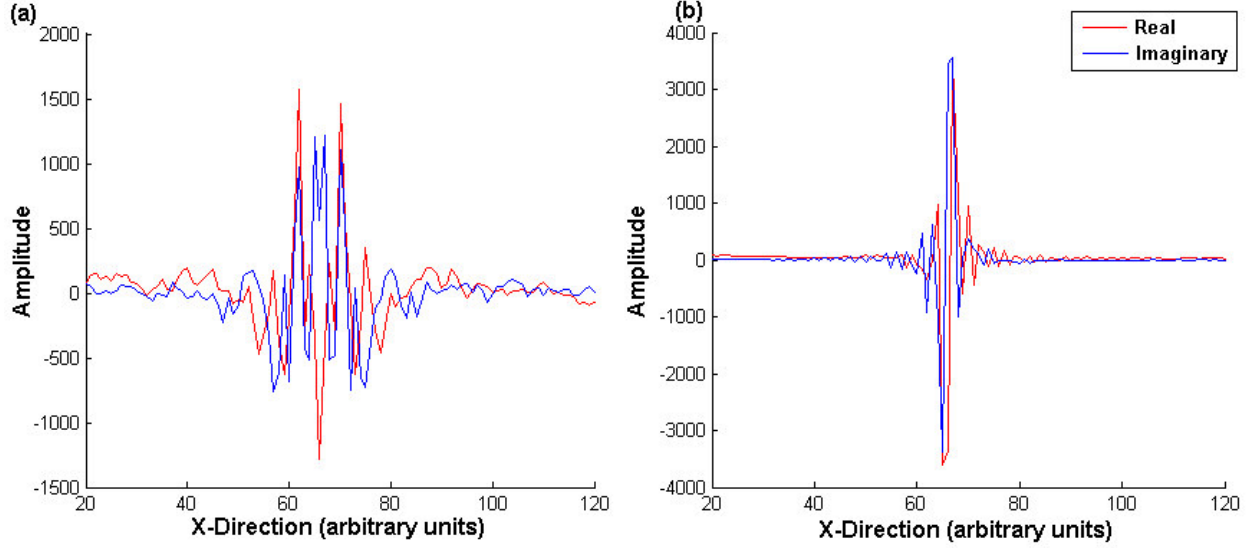


Fig 3. Plots of the real and imaginary parts of the FT of: a) a symmetric function ($Z_{10}^0$) and b) an asymmetric function (astigmatism - $Z_2^{-2}$).

However, it may not be possible to implement an asymmetric function (odd/odd) using a phase only DOE. For the symmetric filter function the convolution of the input wavefront with this function sums weighted wavefront values locally and the re-enforcement or cancellation that results is what generates an error signal for a non-flat input wavefront.

Equation 1 shows the form of the error signal generated by a suitable GPD filter function. From this equation we can see that $d(r)$ will change sign if the sense of the wavefront error is reversed (this follows from the symmetry of $A(\xi)$). In this way the error signal encodes the sense of the error.

The location of the wavefront error is directly related to a $a(r)$ (the transform of $A(\xi)$). If the filter function is concentrated or peaked around the origin (see fig 3) then the position of the wavefront error signal will be located around the point that $a(r)$ is non-zero. Since we intend to design a GPD sensor that operates in the pupil plane there is a 1-1 mapping relationship between the point at which an error signal is detected and the position of the actual error on the intensity image.

The sense and the location of the error could be used to drive a wavefront modulator to correct the wavefront distortions. However, full reconstruction of the wavefront is unnecessary, and in some cases can be detrimental. Therefore even though the required information for wavefront reconstruction is included in the error signal, it is sufficient to operate as a null sensor.

# 3. SIMULATIONS

Computer simulations were conducted to validate the analysis presented here and to explore the possibility of optimisation of the filter function given *a priori* information about the wavefront errors.

Simulations were conducted to look at the intensity images and difference signal generated when an aberrated wavefront was convolved with a user defined diversity function. Fig 4a shows the input wavefront used in one of these simulations created using a mixture of Zernikes with a peak to valley distortion of about 3 waves. Defocus and Spherical Aberration diversity kernels were applied to this wavefront, both with amplitude of $0.5\,\lambda$ and the error signal $d(r)$ computed (fig 4.b and c):
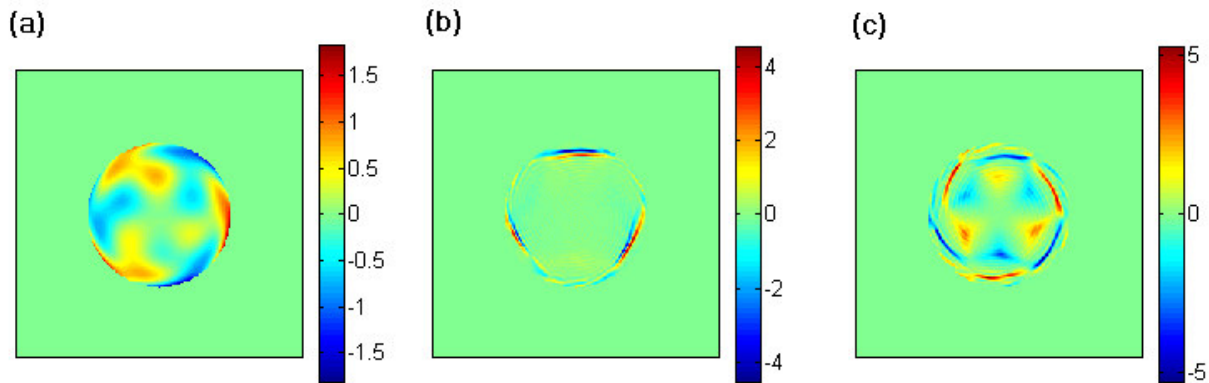


Fig. 4 a. Test wavefront to which was applied two different diversity kernels; 4.b.Defocus and 4.c. Spherical Aberration, both with amplitude $0.5\,\lambda$ .

In 4.a. the scale is waves of wavefront error, whereas in figs 4.b and c. the scale represents the contrast of the error signal. As this figure shows, for the same input wavefront the Spherical Aberration filter produces greater contrast and a signal that more clearly shows the shape of the test wavefront.
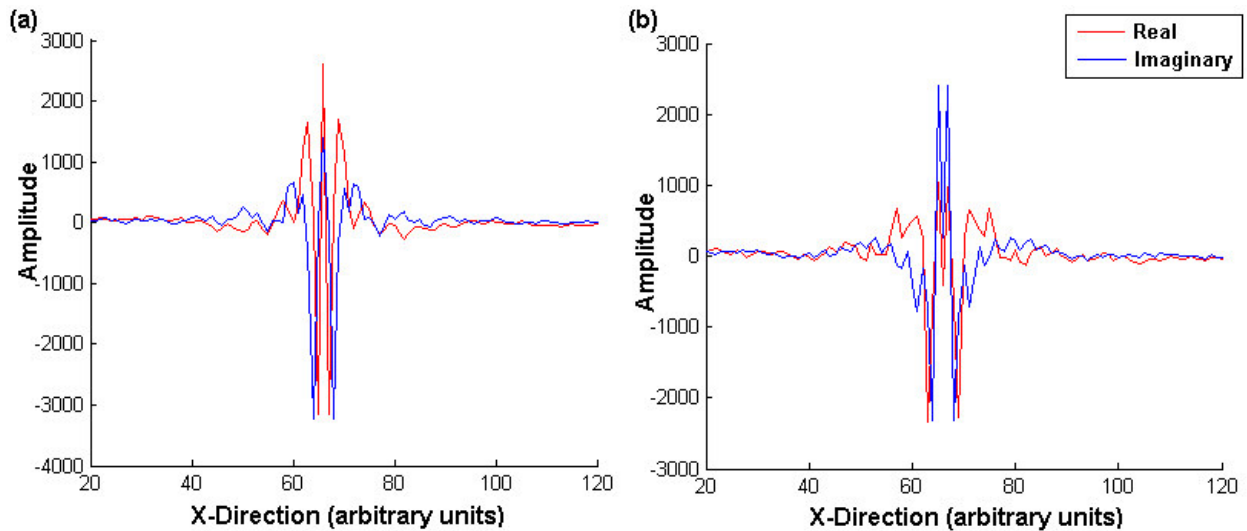


Fig 5: The Real and Imaginary parts of the FT of the filter function for a) Defocus and b) Spherical Aberration.

Fig 5 shows the side lobe of the FT of the two different filter functions used to generate the results shown in fig 4. The intensity images formed in the ±1 diffraction orders (see fig 2) are produced by the convolution of the input

wavefront with the side lobes of the filter function FT. As fig 5 clearly shows, the side lobe in the S.A case is wider than in the defocus case. Therefore, when the input wavefront is convolved with this wider function it will mix the signal over a larger area of the wavefront than the defocus filter will. We would expect therefore that for a given wavefront error the SA filter will produce a larger signal and be more sensitive to small deformations in the wavefront. In fig 4 we see that simulation shows this to be the case.

Numerical experiments were conducted using a plane wave input and a selection of phase diversity kernels with different symmetry properties. These simulations took intensity images places about the image plane. Simulations using an even symmetry filter function and a plane wave input generated zero error signal (to within rounding error - $10^{-14}$). Fig.6(a) shows the difference $d(r)$ with an even symmetry filter function and a distorted input wavefront. In fig. 6(b) a mixed symmetry filter comprising defocus and astigmatism is used with a plane wave input and it is clearly seen that a large difference signal is produced.
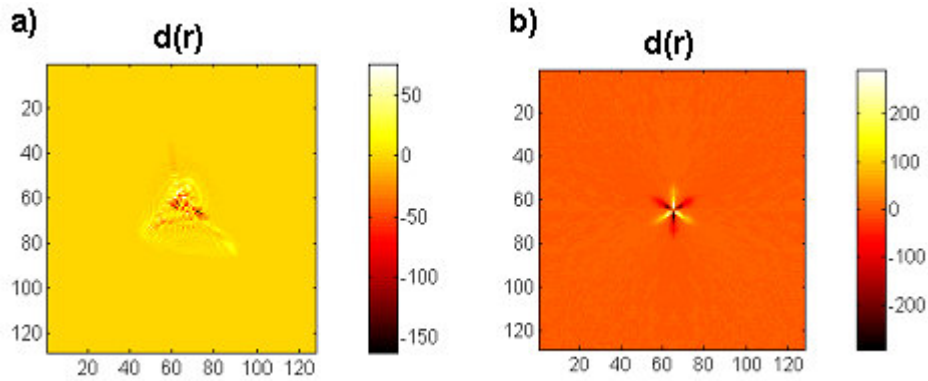


Fig. 6. Difference between ±1 diffraction order intensity images about the image plane for (a) even symmetric $Z_2^0$ filter with a distorted input wavefront (b) Mixed symmetry $Z_2^0 + Z_3^{-3}$ filter with a plane wave input.

These numerical experiments also showed that for a wavefront with a $\pi$ phase step the difference function was also zero. This means that the GPD wavefront sensor will be insensitive to steps in the wavefront phase that are integral numbers of $\pi$. These discontinuities are effectively a local change of sign of the wavefront. Preservation of these phase steps is essential to preserve band-limited behaviour [10]. This is unimportant for astronomy but potentially important for metrology applications. These numerical experiments have demonstrated how filter function with different symmetry properties may be used to create a useful null wavefront sensor.

It may be desirable in some cases (e.g. metrology applications) to reconstruct the wavefront so we ran further simulations to look at wavefront reconstruction under different phase diversity kernels. In a GPD wavefront sensing system it is possible to use aberrations other than defocus to provide the phase diverse data. In cases where *a priori* information about wavefront errors is available, this information can be used to choose a diversity kernel appropriate to the application. Poor choice can easily lead to poor performance. Our simulations have shown that it is better to use a symmetric phase diversity function (such as defocus or spherical aberration) unless it is explicitly known that asymmetric errors (like astigmatism) are expected. We used an error-reduction algorithm, a signal to noise ratio of 30 and Poisson distributed noise in all of the reconstruction simulations. Fig 7 is a plot of error against iteration number and shows the convergence of the algorithm for 3 different diversity kernels, $Z_2^0, Z_4^0, Z_{10}^0$.
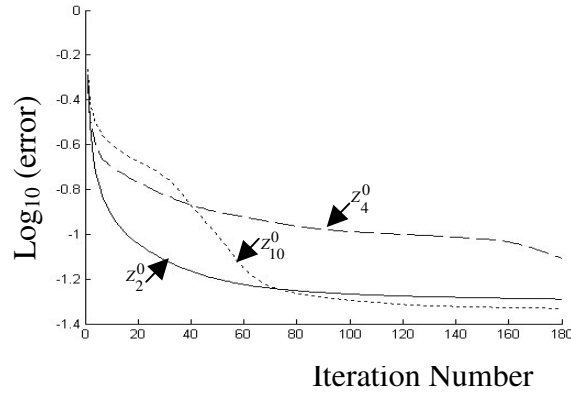
Fig 7. $Log_{10}$(error) vs. Iteration number for a numerical wavefront reconstruction using 3 different phase diversity kernels, $Z_2^0, Z_4^0, Z_{10}^0$

The main purpose of fig 7 is to demonstrate that given the same distorted input wavefront the convergence behaviour of each kernel was different. This shows that there is the potential to optimise GPD filter functions for particular applications and thus has greater sensitivity to the most common errors present in any system.

## 4. EXPERIMENTAL SET-UP AND RESULTS

The next step is to create new diffraction gratings with suitable filter functions and construct the wavefront sensor. New DOE have been designed and their fabrication is in hand. To begin with a quadratically distorted (defocus) diffraction grating was used, since this was known to work in the DPD sensor it could be used as a 'ground truth' test of the new system. The GPD system not only will comprise new and different DOE's, it also requires a new form of data analysis to avoid the constraints of the Green's function solution used previously. Phase retrieval software was developed using a Gureyev-Nugent (GN) algorithm [11, 12] to obtain the wavefront reconstruction from the intensity images created by the grating. This method is based on the decomposition of the ITE into Zernike polynomials. This algorithm works well in the presence of non-uniform illumination [12]. Therefore the GPD wavefront sensor should be able to cope with scintillated wavefronts.

A single mode fibre was mounted on a computer controlled translation stage to be used as a point source. A quadratically distorted (defocus) DOE, with a focal length of ±4m, was mounted together with a 60mm focal length achromat, and a CCD camera was placed to focus the source onto the camera. Under these circumstances the point source was then translated about the focal position and the intensity images in the ±1 diffraction orders were recorded. These images were then analysed using the GN algorithm and the defocus coefficient was measured. This data was then plotted and compared to the values calculated from equation 2:

$$s = -\frac{r^2 \Delta z}{2z^2} + \frac{r^2 (\Delta z)^2}{2z^3} - \dots \dots \tag{2}$$

Where $s$ is the sag produced by the displaced source, $r$ is the radius of the lens, $\Delta z$ is the small axial shift of the source from focus and $z$ is the distance between the object and the lens when the source is in focus. Higher order terms than the ones shown in equation 2 have been neglected. Fig 7 is a plot of the calculated sag from equation 2 and the measured defocus values. The focal distance (z) was found to be 783.5 mm from the lens, this distance is marked on the graph by the black dotted lines.
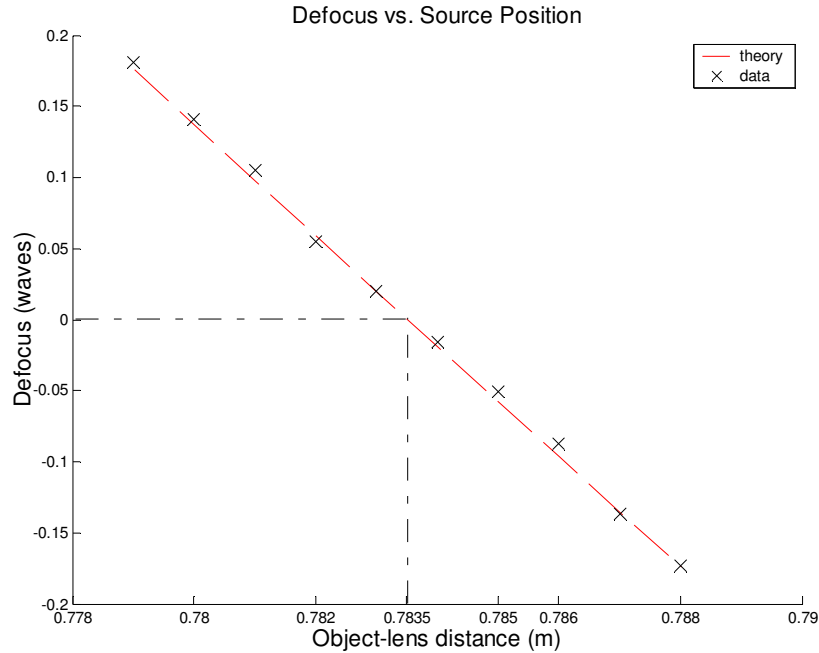
Fig 8: Graph showing the calculated defocus values (theory) and the experimental data.

As Fig 8 clearly shows, use of the GN algorithm has given phase retrieval results which are very close to the theoretical values. The total root mean square (rms) error between the calculated and measured defocus values is 0.005257waves which corresponds to an accuracy of $\lambda/190$. Whilst this does not yet match previous best results from the Green's function analysis [6], this result shows that the GN can be used to give accurate phase retrieval results. We will go on to use DOE's with different filter functions to create a GPD wavefront sensor.

Our results have shown that it will be possible to build a GPD null sensor using filter functions that may include, but will not be limited to, defocus. Any filter function which satisfies the symmetry conditions may be used, and it should be possible to optimise the choice of function for a given application if *a priori* knowledge of the wavefront errors is available. The GPD wavefront sensor will be robust, compact, better suited to dealing with scintillated and discontinuous wavefronts and will therefore be suitable for a wider range of applications.

Future work will include the use of a Mach-Zehnder Interferometer which has been built to act as a test bed for the GPD sensor, and also to characterise the membrane Deformable Mirrors (DMs) manufactured by Flexible Optical. This system is shown in fig 9:
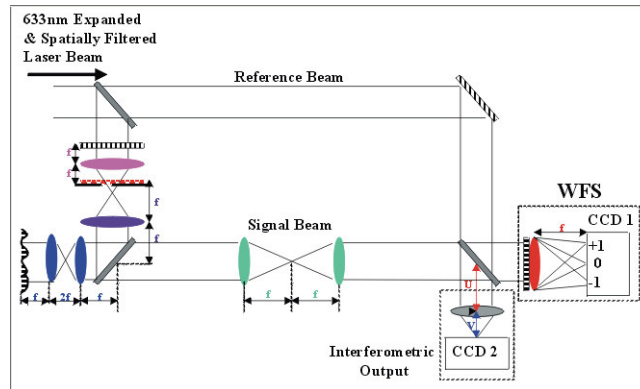


Fig. 9 A Mach-Zehnder Interferometer with a both a GPD wavefront sensor and a second CCD to capture the interferogram for standard forms of analysis.

This system will allow us to test the GPD sensor output against standard interferometric measurements. In addition to this DOE's can be placed in the signal arm, with a spatial filter to only allow one diffraction order to pass through the system, to set up test wavefronts with known profiles. These DOE's will also act as static phase screens that the DM's can be used to correct, and if more DOE's are added can be converted into a Multi Conjugate Adaptive Optics test bed. Comparison results of the GPD sensor with different filter functions against standard interferogram analysis will be given in future publications.

## REFERENCES

1. Barty, A., et al., *Quantitative Optical Phase Microscopy.* Optics Letters, 1998. **23**(11): p. 817-819.
2. Roddier, F., *Curvature sensing and compensation: a new concept in adaptive optics.* Applied Optics, 1988. **27**(7): p. 1223-1225.
3. Blanchard, P.M., et al., *Phase-diversity wave-front sensing with a distorted diffraction grating.* Applied Optics, 2000. **39**(35): p. 6649-6655.
4. Woods, S.C. and A.H. Greenaway, *Wave-front sensing by use of a Green's function solution to the intensity transport equation.* Journal of the Optical Society of America A-Optics & Image Science, 2003. **20**(3): p. 508-12.
5. Gonsalves, R.A. *Perspectives on Phase Diversity*. in *the workshop on wavefront sensing and controls*. 2000. Hawaii.
6. Djidel, S. and A.H. Greenaway. *Nanometric wavefront sensing*. in *3rd International Workshop on Adaptive Optics in Industry and Medicine*. 2002: Starline Printing Inc.
7. Dayton, D.C., et al., *Theory and laboratory demonstrations on the use of a nematic liquid-crystal phase modulator for controlled turbulence generation and adaptive optics.* Applied Optics, 1998. **37**(24): p. 5579-89.
8. Kirby, K. and G. Love, *Fast, large and controllable phase modulation using dual frequency liquid crystals.* Optics Express, 2004. **12**(7): p. 1470-1475.
9. Campbell, H.I., et al., *Generalised Phase Diversity for Wavefront Sensing.* Optics Letters, 2004. **Accepted for publication**.
10. Dillon, C. and et al. *The Treatment of Branch Cuts in Adaptive Optics*. in *This Proceedings*. 2004.
11. Gureyev, T.E., A. Roberts, and K.A. Nugent, *Phase retrieval with the transport-of-intensity equation: matrix solution with use of Zernike polynomials.* Journal of the Optical Society of America A: Optics and Image Science, and Vision, 1995. **12**(9): p. 1932.
12. Gureyev, T.E. and K.A. Nugent, *Phase retrieval with the transport-of-intensity equation. II. Orthogonal series solution for nonuniform illumination.* Journal of the Optical Society of America A: Optics and Image Science, and Vision, 1996. **13**(8): p. 1670.